Supporting Information

Ta_2O_5/SiO_2 Multicomponent Dielectrics for Amorphous Oxide TFTs

Jorge Martins [1,*], Asal Kiazadeh [1], Joana V. Pinto [1], Ana Rovisco [1], Tiago Gonçalves [1], Jonas Deuermeier [1], Eduardo Alves [2], Rodrigo Martins [1], Elvira Fortunato [1] and Pedro Barquinha [1,*]

[1] i3N/CENIMAT, Department of Materials Science, NOVA School of Science and Technology and CEMOP/UNINOVA, NOVA University Lisbon, Campus de Caparica, 2829-516 Caparica, Portugal; a.kiazadeh@fct.unl.pt (A.K.); jdvp@fct.unl.pt (J.V.P.); a.rovisco@campus.fct.unl.pt (A.R.); td.goncalves@campus.fct.unl.pt (T.G.); j.deuermeier@campus.fct.unl.pt (J.D.); rfpm@fct.unl.pt (R.M.); emf@fct.unl.pt (E.F.)

[2] IPFN, Instituto Superior Técnico, University of Lisbon, EN 10, km 139,7 2695-066 Bobadela, Portugal; ealves@ctn.tecnico.ulisboa.pt

* Correspondence: jds.martins@campus.fct.unl.pt (J.M.); pmcb@fct.unl.pt (P.B.)

Compositional and structural analysis of the multicomponent dielectrics by Rutherford backscattering spectrometry (RBS), spectroscopic ellipsometry (SE), X-ray difraction (XRD) and Atomic Force Microscopy (AFM).

Table S1. Molar concentrations and film density obtained by RBS analysis of Ta_2O_5, SiO_2 and Ar in the thin films deposited using different powers in the Ta_2O_5 and SiO_2 targets. Thickness of the films extracted by SE from [53].

Ta_2O_5 power (W)	Density (10^{15} atm/cm^2)	SiO_2 power (W)	Ta_2O_5 (mol.%)	SiO_2 (mol.%)	Ar (at.%)	Norm. Ta_2O_5 (mol.%)	Norm. SiO_2 (mol.%)	Thickness (nm)
50	1668	150	37.5	59.1	3.4	39	61	243
75	1495	150	57.6	38.6	3.8	60	40	206
100	1796	150	65.7	30.0	4.3	69	31	245
125	1712	150	70.6	25.0	4.5	74	26	233
150	1923	150	71.7	23.9	4.4	75	25	257
100	1855	-	94.5	-	5.5	100	0	232

While the Ar content is relatively similar across the film compositions presented in Table S1, a small tendency is still noticeable with the increase of the Ta_2O_5 content. The total atomic fraction of Ar incorporated in the material, x_{Ar}, can be described as the sum of the fractions incorporated in both the Ta_2O_5 material and the SiO_2 material, as shown in Equation (1),

$$x_{Ar} = x_{Ar@Ta_2O_5} x_{Ta_2O_5} + x_{Ar@SiO_2} x_{SiO_2} \quad (1)$$

where $x_{Ta_2O_5}$ and x_{SiO_2} are the non-normalized molar fractions of Ta_2O_5 and SiO_2, respectively, and $x_{Ar@Ta_2O_5}$ and $x_{Ar@Ta_2O_5}$ are the fraction of Ar incorporated in each of these materials, respectively. Knowing that the fractions of each material add to 1, as shown in Equation (2), Equation (1) can then be rewritten as Equation (3), describing the Ar content as a function of the Ta_2O_5 content, as presented in Figure S1. Trough linear fitting of this data, the fractions of Ar incorporation in each material,

$x_{Ar@SiO_2}$ and $x_{Ar@Ta_2O_5}$, are calculated as 1.9 % and 5.7 %, respectively, proving that Ta_2O_5 is much more prone for Ar incorporation than SiO_2.

$$1 = x_{Ar} + x_{Ta_2O_5} + x_{SiO_2} \tag{2}$$

$$x_{Ar} = \left(\frac{x_{Ar@Ta_2O_5} - x_{Ar@SiO_2}}{1 + x_{Ar@SiO_2}}\right) x_{Ta_2O_5} + \frac{x_{Ar@SiO_2}}{1 + x_{Ar@SiO_2}} \tag{3}$$

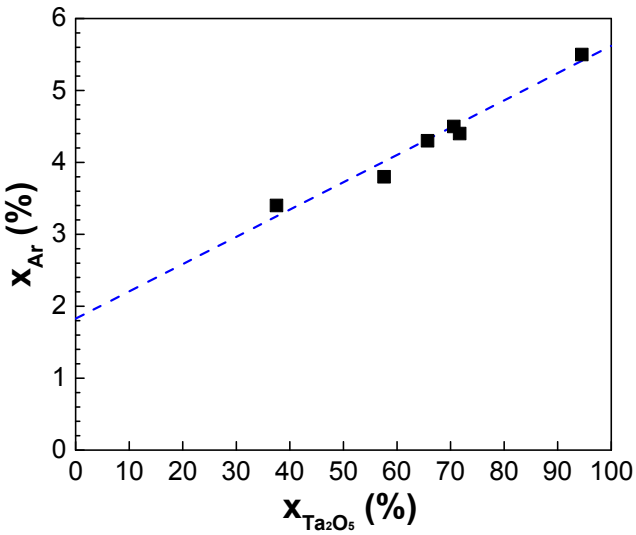

Equation	y = a + b*x
Plot	B
Weight	No Weighting
Intercept	1.8278
Slope	0.03793
Residual Sum of Squares	0.07577
Pearson's r	0.98497
R-Square(COD)	0.97017
Adj. R-Square	0.96023

Figure S1. Ar concentration as a function of the Ta_2O_5 concentration.

Capacitance-Voltage characteristics of MIS structures.

C-V curves measured from the MIS structures. The thicknesses (as described in Table S1) and MIS areas are also included in the figure.

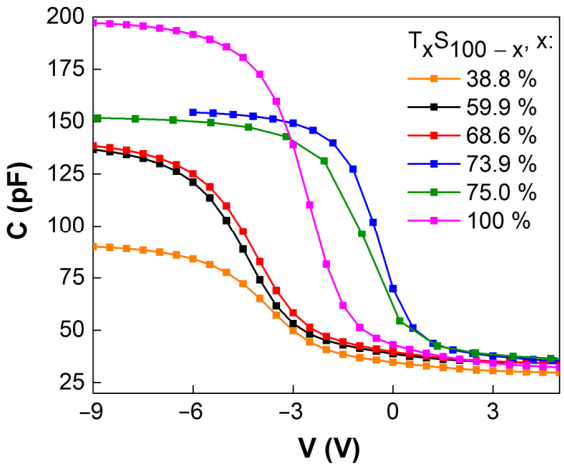

Ta_2O_5 (mol.%)	SiO_2 (mol.%)	Thickness (nm)	Area (cm^2)
39	61	243	1.60×10^{-3}
60	40	206	1.88×10^{-3}
69	31	245	1.88×10^{-3}
74	26	233	1.88×10^{-3}
75	25	257	1.88×10^{-3}
100	0	232	1.88×10^{-3}

Figure S2. C-V curves of the MIS employing the T_xS_{100-x} dielectric layers. The composition and geometrical properties of the MIS are presented in the table.

Anomalous threshold voltage shift (ΔV_{th}) during PGBS, recovery and NGBS.

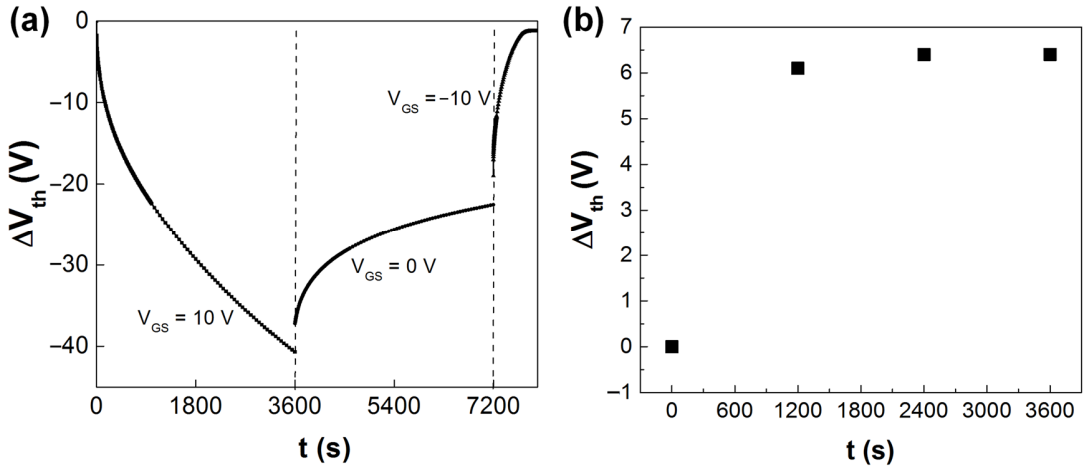

Figure S3. (a) V_{th} shift measured during gate biasing with V_{GS} = 10 V, V_{GS} = 0 V and V_{GS} = −10 V, sequentially, for the $T_{69}S_{31}$ composition. (b) V_{th} shift measured during negative gate biasing with V_{GS} = −10 V for an as-fabricated device with the $T_{39}S_{61}$ composition.

While the ΔV_{th} shift (observed only during the first minutes) during NGBS in as-fabricated devices is much lower than during PGBS, the channel is depleted during NGBS and thus only charges in the overlap areas between the gate and the source and drain electrodes are expected to respond to the biasing, making a direct comparison of these shift magnitudes unfeasible.

Power law time dependency of ΔV_{th} during positive gate bias stress

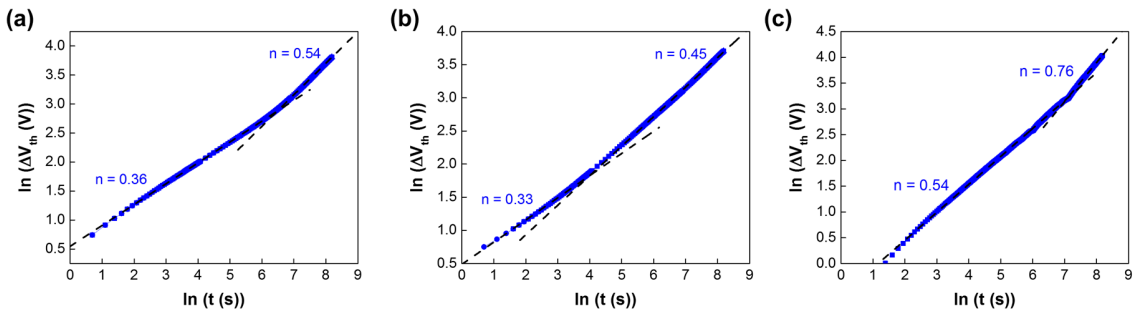

Figure S4. ΔV_{th} during positive gate bias stress (V_{GS} = 10 V) for the (a) $T_{60}S_{40}$, (b) $T_{69}S_{31}$ and (c) $T_{69}S_{31}/SiO_2$ compositions, showing power law time dependencies.